Current Applied Physics xxx (2013) 1–6

Contents lists available at SciVerse ScienceDirect

Current Applied Physics

journal homepage: www.elsevier.com/locate/cap

Two-step fabrication of ZnO nanosheets for high-performance VOCs gas sensor

Shao-Lin Zhang [a], Jeong-Ok Lim [b], Jeung-Soo Huh [c], Jin-Seo Noh [a], Wooyoung Lee [a,*]

[a] Department of Materials Science and Engineering, Yonsei University, Seoul 120749, Republic of Korea
[b] Biomedical Research Institute, Kyungpook National University, Daegu 702701, Republic of Korea
[c] School of Materials Science and Metallurgy, Kyungpook National University, Daegu 702701, Republic of Korea

ARTICLE INFO

Article history:
Received 7 November 2012
Accepted 28 December 2012
Available online xxx

Keywords:
Zinc oxide
Nanosheets
Volatile organic compounds
Gas sensor

ABSTRACT

Sheet-like ZnO nanostructure was successfully synthesized through a simple, cost-effective, and low-temperature sonochemical process followed by an etching treatment in an alkali environment at room temperature without any catalyst, template, or seed layer. The morphology and crystallinity of the products were examined by X-ray diffraction (XRD) analysis, scanning electron microscopy (SEM) and transmission electron microscopy (TEM). The as-prepared nanosheets with high purity were single crystals and well-dispersed. A possible formation mechanism of ZnO nanosheets was proposed based on the experimental results. Micro gas sensor fabricated from the as-prepared ZnO nanosheets were tested to different concentration of volatile organic compounds (VOCs) gases. The gas-sensing results revealed that ZnO nanosheets-based micro sensor exhibited high sensitivity to acetaldehyde and formaldehyde with response time within 10 s and the detection limit down to 50 ppb. The excellent sensing property of ZnO nanosheets is mainly attributed to their large specific area, accessible surface, and less agglomerated configuration.

1. Introduction

Since the gas sensing capability of metal oxide semiconductors was revealed in the 1960s [1], great attention has been paid to the investigation of gas sensors based on various semiconducting metal oxides, such as SnO_2, TiO_2, In_2O_3, WO_3, and ZnO [2–4]. As one of the key n-type multifunctional semiconductors, ZnO has been proved to be a primary material to develop practical gas sensors owing to its low-cost, facile preparation process, and high chemical and physical stability [5,6]. Along with the progress of gas sensor research, it has been found nanostructures with small crystal size, large surface-to-volume ratio and high density of surface active sites possess much more excellent sensing property compared with their bulk counterparts. Thus considerable attention has been given to gas sensors utilizing ZnO nanoparticles and one-dimensional (1D) ZnO nanomaterials (e.g., nanorods, nanowires, nanotubes, and nanobelts) in the last decade [7,8]. Recently, gas sensors based on two-dimensional (2D) nanostructures such as nanosheets, nanoflakes, and nanoplates have begun to attract the interest of researchers due to the distinctive structure and high sensing performance [9–12]. Zhang et al. synthesized porous ZnO nanosheets through a low-temperature hydrothermal process followed by annealing treatment. The obtained ZnO nanosheets exhibited an ultrahigh response to ethanol at 400 °C [13]. Chen et al. fabricated ZnO polygonal nanoflakes by the microwave hydrothermal method. Comparative tests demonstrated a gas sensor based on ZnO nanoflakes was more excellent than that based on ZnO nanoparticles in NO_2 sensing performance [14]. However, compared to ZnO nanoparticles and 1D nanostructures, controlled synthesis of 2D ZnO nanostructures and research on their gas sensing properties are still at an early stage. Thus, an in-depth research on the synthesis of ZnO nanosheets and exploration of their sensing properties are necessary.

The indoor pollution of volatile organic compounds (VOCs), such as benzene, toluene, acetaldehyde, and formaldehyde, has been recognized as the principal cause of many diseases including asthma, emphysema, allergies, and cancer, and received more and more public concern these days [15]. However, the detection of indoor VOCs, especially, in low concentration using conventional sensing materials still remains a challenge, often failing to meet the ultralow indoor leakage standard of VOCs. It is considered that 2D nanostructures may have a potential to develop high performance VOCs gas sensors owing to their large surface-to-volume ratio, less agglomerated configuration, and distinct sheet-like structure.

* Corresponding author. Tel.: +82 2 2123 2834; fax: +82 2 312 5375.
E-mail address: wooyoung@yonsei.ac.kr (W. Lee).

1567-1739/$ – see front matter © 2013 Elsevier B.V. All rights reserved.
http://dx.doi.org/10.1016/j.cap.2012.12.021

In the present study, dispersive single-crystalline ZnO nanosheets were synthesized through a two-step process, which included the fabrication of ZnO nanorods by a simple, cost-effective, and low-temperature sonochemical method, and etching treatment to etch nanorods into nanosheets in an alkali environment at room temperature without any catalyst, template, or seed layer. The sensor fabricated from the ZnO nanosheets showed excellent sensing characteristics to acetaldehyde and formaldehyde, in terms of high sensitivity, and small response and recovery time. Most surprisingly, the detection limit was as low as 50 ppb.

2. Experimental details

2.1. Two-step fabrication and characterization of ZnO nanosheets

In the first step, ZnO nanorods as precursor were synthesized by the sonochemical method at room temperature using zinc nitrate hydrate ($Zn(NO_3)_2 \cdot 6H_2O$) and hexamethylenetetramine (HMT, $C_6H_{12}N_4$, also known as methenamine) as starting materials without any surfactant, catalyst or template. In a typical process, a 100 ml aqueous solution of $Zn(NO_3)_2 \cdot 6H_2O$ and a 100 ml aqueous solution of HMT at equivalent concentrations (0.025 M) were mixed together under vigorous magnetic stirring. The solution was subsequently irradiated by intense ultrasound (500 W, 20 kHz) for 90 min under ambient conditions. The ultrasonic treatment was performed using an ultrasonic processor (VCX 750, Sonics & Materials) with a 0.5-inch horn made of a titanium alloy. The transparent solutions changed to white suspensions after irradiation. The white precipitate was then separated from the solution by centrifuge, washed with distilled water and ethanol five times each to remove ionic impurities, and finally dried in a vacuum for 12 h at room temperature.

ZnO nanosheets were subsequently fabricated by chemical etching of the ZnO nanorods obtained from the above-mentioned process. The ZnO nanorods powder was mixed with a proper volume of ethanol and vigorously stirred for 10 min. The resulting suspension was then added dropwise into 50 ml NaOH solution with a concentration of 1.5 M within 10 min at room temperature. After constant magnetic stirring for 24 h, the white product was centrifuged, washed, and dried in a vacuum, and finally ZnO nanosheets were obtained.

The ZnO nanorods and nanosheets were characterized by X-ray diffraction (XRD, Cu Kα) to observe the structural nature. The XRD patterns were recorded from 10° to 80° (2θ) at a scanning step of 0.02°. The morphology of the product was analyzed by field-emission scanning electron microscopy (FE-SEM, Hitachi S-4300) operated at 15 keV. The transmission electron microscopy (TEM) and selected area electron diffraction (SAED) images were obtained using a Hitachi H7600 transmission electron microscope at an acceleration voltage of 100 kV.

2.2. Sensor fabrication and measurement

The micro sensor substrate was developed using MEMS technology to minimize the power consumption of the sensor. The micro substrates were fabricated in 300-μm-thick, 4 inch Si wafers. A Si_3N_4 film was first deposited on the wafers by low pressure chemical vapor deposition (LPCVD). Then, platinum (Pt) was deposited by sputtering with a patterned mask. After removing the mask, a patterned micro-heater and electrode were obtained. A silicon dioxide (SiO_2) passivation layer was deposited on top of the metallized Pt to electrically isolate the sensing electrode from the micro-heater. The dimensions of the substrate were 1.8 mm × 1.8 mm with a 400 μm × 400 μm sensing area, as shown in Fig. 1(a). The gap distance between the two electrodes was 70 μm, and the resistance of the micro-heater was about 30 Ω.

The obtained ZnO nanosheets powder was mixed with ethyl cellulose and α-terpineol (weight ratio 1:20) to form a homogeneous paste. The paste was then coated onto the MEMS substrate by a dropping method. Subsequently, the fabricated MEMS sensor was dried at 90 °C for 2 h and annealed at 600 °C for 1 h. The drying process was used to prevent a potential explosion during subsequent high temperature heating, while the annealing treatment was used to remove the impurities and improve the stability of the sensors. A cross-sectional view of the MEMS sensor after coating ZnO nanosheets is shown in Fig. 1(b).

The prepared MEMS sensor was soldered to a tetrapod holder by a wire bonding process and covered by a meshed cap. Then, the sensor was placed into a test chamber with a total volume of 5 cm^3. Synthetic dry air at a constant flow rate of 250 sccm acted as a carrier gas. Manufactured standard VOCs gases (acetaldehyde and formaldehyde) were diluted with nitrogen (Daehan Gas Co., Ltd.) for the desired concentrations, and were used as target gases. The accurate concentration control of the VOCs gases was enabled using a combination of certified cylinders and a mixing system equipped with mass flow controllers and mass flow meters. The sensitivity is defined as

$$S(\%) = \frac{R_g - R_a}{R_g} \times 100\% \quad (1)$$

where R_a and R_g represent the resistance of the MEMS sensor upon exposure to air and a target gas, respectively. The response and

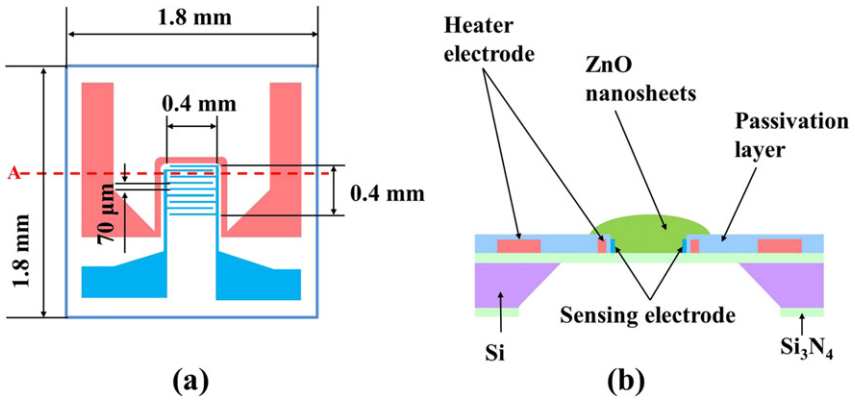

Fig. 1. (a) Schematic diagram of the micro sensor substrate; (b) cross-sectional view of the micro sensor after coating sensing material.

Please cite this article in press as: S.-L. Zhang, et al., Two-step fabrication of ZnO nanosheets for high-performance VOCs gas sensor, Current Applied Physics (2013), http://dx.doi.org/10.1016/j.cap.2012.12.021

recovery time are defined as the time taken by the sensor to achieve 90% of the total resistance change in the respective case of adsorption and desorption.

3. Results and discussion

3.1. Characterization and formation mechanism of ZnO nanosheets

The crystal structure and the phase purity of the ZnO nanorods and the final ZnO nanosheets were characterized by XRD, and the resultant XRD patterns are shown in Fig. 2. All peaks of the both materials can be indexed to hexagonal wurtzite ZnO with a lattice constant of $a = 0.325$ nm and $c = 0.521$ nm, which are consistent with the value in the standard card (JCPDS card No. 36-1451). The strong diffraction peaks indicate that the product is in a highly crystallized form. No characteristic peaks for any other impurities were observed, suggesting both samples have high purity. From the XRD observation, it is found that the crystal structure of the product is kept unchanged after etching treatment. The crystallite size of ZnO nanosheets was calculated from X-ray line broadening analysis using the Scherrer equation, $D = 0.89\lambda/(\beta\cos\theta)$, where D is the average crystal size in nm, λ is the X-ray wave length (Cu Kα: 0.15406 nm), β is the full width at half-maximum (FWHM) of the peak, and θ is the corresponding Bragg diffraction angle. The mean crystallite size of the ZnO nanosheets was calculated to be approximately 68 nm.

The morphology of the as-prepared ZnO nanosheets was characterized via FE-SEM and TEM. Representative images obtained with gradually increasing a magnification are displayed in Fig. 3. Fig. 3(a) is a low-magnification FE-SEM image, indicating that well-dispersed ZnO nanosheets was synthesized on a large scale through this synthesis method. Its magnified image (Fig. 3(b)) reveals the nanosheets have a size of about 200–400 nm and edge thickness of about 10–60 nm. These values are close to the crystallite size of 68 nm previously calculated from the XRD measurement. The composition of the nanosheets was further investigated by the X-ray energy dispersive spectroscopy (EDS) as shown in the inset of Fig. 3(b). From the EDS analysis, the atomic ratio of Zn and O in the ZnO nanosheets was calculated to be approximately 1, matching well with the nominal stoichiometry. Furthermore, no impurity signals are observed other than Pt. The Pt signal originates from a Pt film coated on the sample for SEM observation. A detailed structural analysis of individual nanosheets was conducted using TEM and SAED. Fig. 3(c) presents a typical low-magnification TEM image of the well-dispersed ZnO nanosheets. The TEM image confirms the well-defined sheet-like structure of the nanosheets. The nanosheets have unique features such as an irregular thickness and a serrated fringe, which contribute to the generation of abundant defects on the surface of nanosheets. It is believed that the existence of surface defects may facilitate the absorption of oxygen species and thus enhance the gas sensing property of ZnO nanosheets. The corresponding high-resolution TEM (HRTEM) image (Fig. 3(d)) and SAED pattern verify that the ZnO nanosheets are single-crystalline in nature.

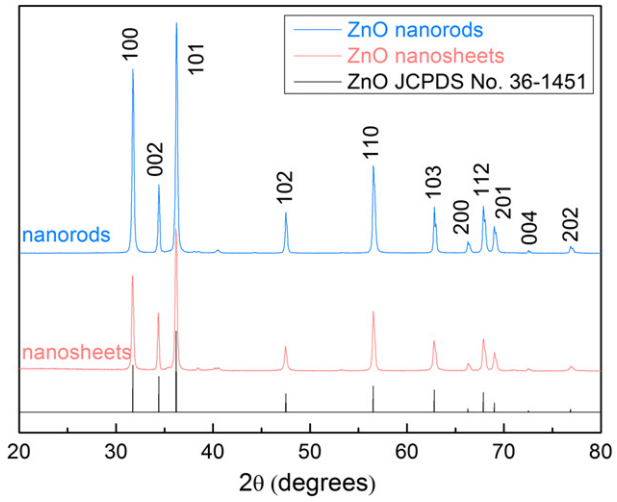

Fig. 2. XRD patterns of ZnO nanorods and nanosheets, along with a standard JCPDS pattern for ZnO.

To understand the mechanism of ZnO nanosheets formation, some controlled etching experiments have been carried out with different treatment times. Fig. 4(a) displays the morphology of as-prepared ZnO nanorods before etching. It is observed that uniform nanorods with a diameter of about 150 nm and a length of about 600 nm were fabricated on a large scale by the sonochemical process. The tips of these nanorods are hexagon-shaped flat planes. Fig. 4(b)–(e) show the morphology evolution of the ZnO nanorods as a function of etching time (3 h, 6 h, 14 h, and 24 h) in an alkali environment. It is evident that the etching time plays a key role in the formation of ZnO nanosheets. After etching for 3 h (Fig. 4(b)), hollow structures appear on the tips of most ZnO nanorods. No obvious etching effect is observed on the lateral walls of nanorods, indicating the etching effect takes place preferentially. Extending the etching time to 6 h, the hollow structure propagates into the inner part of the nanorods and results in a serrated fringe on the tip of nanorods. It is also found that side walls becomes broken for prolonged etching. The break-down of side walls induced by the over-etching is observed for etching time longer than 14 h, and well-developed ZnO nanosheets are finally formed after 24 h etching.

On the basis of the above experimental observation, the possible mechanism for the formation of ZnO nanosheets is schematically presented in Fig. 4(f). When the ZnO nanorods are immersed in alkali solution, ZnO is etched by a reaction with the OH^- anions to form soluble hydroxyl complex according to the reaction equation as follows [16–18],

$$ZnO + H_2O + 2OH^- \leftrightarrow Zn(OH)_4^{2-} \quad (2)$$

The etching starts from the tip of the nanorods and propagates toward their bottom (Fig. 4(b)). The preferential etching in the central part of the nanorods may be due to the rich-existence of defects in the core of nanorods [19–21], which is attributed to the distinct ultrasonic growth mechanism of ZnO nanorods. The ultrasonication during growth is known to greatly increase the nanorods growth rate and prone to generate abundant defects in the central part of nanorods. At a certain etching time, the cores of nanorods are fully dissolved without attacking side faces, leaving behind a tubular structure (Fig. 4(c)). When the etching time further increases, the dissolution of the side walls starts, but it proceeds non-simultaneously due to the inhomogeneous distribution of the active defects in side walls. As a result, quasi sheet-like nanostructures are formed at this stage (Fig. 4(d)). It should be noted that the complete dissolution of nanorods does not happen in this process. This is because the reverse reaction of Equation (2) becomes dominant as the concentration of $Zn(OH)_4^{2-}$ increases. This dominance of the reverse reaction at a longer etching time spontaneously controls the further etch-off of side walls and finally results in ZnO nanosheets (Fig. 4(e)).

3.2. VOCs gas sensing properties of the ZnO nanosheets

The gas sensing properties of ZnO nanosheets are in general based on n-type surface-dominant mechanism, in which adsorption

Please cite this article in press as: S.-L. Zhang, et al., Two-step fabrication of ZnO nanosheets for high-performance VOCs gas sensor, Current Applied Physics (2013), http://dx.doi.org/10.1016/j.cap.2012.12.021

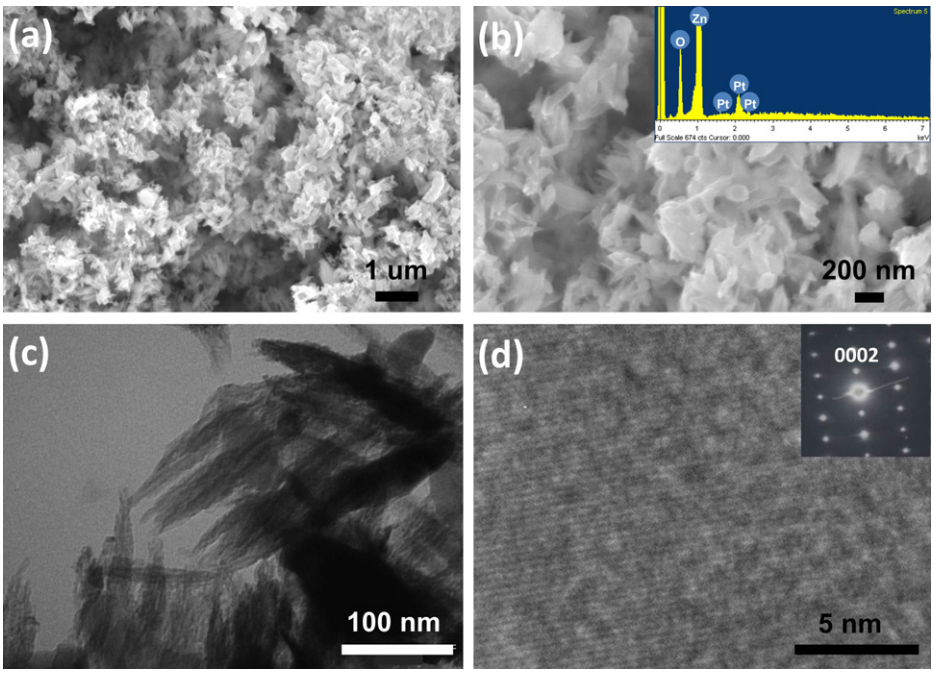

Fig. 3. Morphology of the ZnO nanosheets, (a) low-magnification FE-SEM image; (b) high-magnification FE-SEM image, the inset is the corresponding EDS spectrum; (c) TEM image; (d) HRTEM image, the inset is the corresponding SAED pattern.

and desorption processes occur at the surface of sensing materials. When the nanosheets sensor is exposed to air, oxygen molecules are absorbed onto the surface of the ZnO nanosheets and transformed to O_2^-, O^-, or O^{2-} depending on the operation temperature [22]. The absorption of oxygen traps free electrons from the conduction band of ZnO nanosheets and causes the increase of resistance of the sensor. When the sensor is exposed to a reducing gas like VOCs gases, the VOCs gas molecules react with the absorbed oxygen anions and release the trapped electrons to the conduction band, leading to a decrease in the resistance. Thus, the active surface area and surface status of the sensing material play a crucial role in the gas sensing performance. ZnO nanosheets with large surface area and abundant surface defects is expected to show excellent sensing performance.

For the investigation of the gas sensing properties of the ZnO nanosheets, the optimum operation temperature should be determined at the very first. For this, the average sensitivity of the ZnO nanosheets sensor to 1 ppm of formaldehyde and acetaldehyde was measured as a function of the operation temperature and the results are shown in Fig. 5. The sensitivities to both VOCs target gases continuously increase with increasing the operation temperature until they reach their maximum at 220 °C. A further increase of the temperature gives rise to a downturn of the sensitivities. The maximum sensitivities to 1 ppm of formaldehyde and acetaldehyde

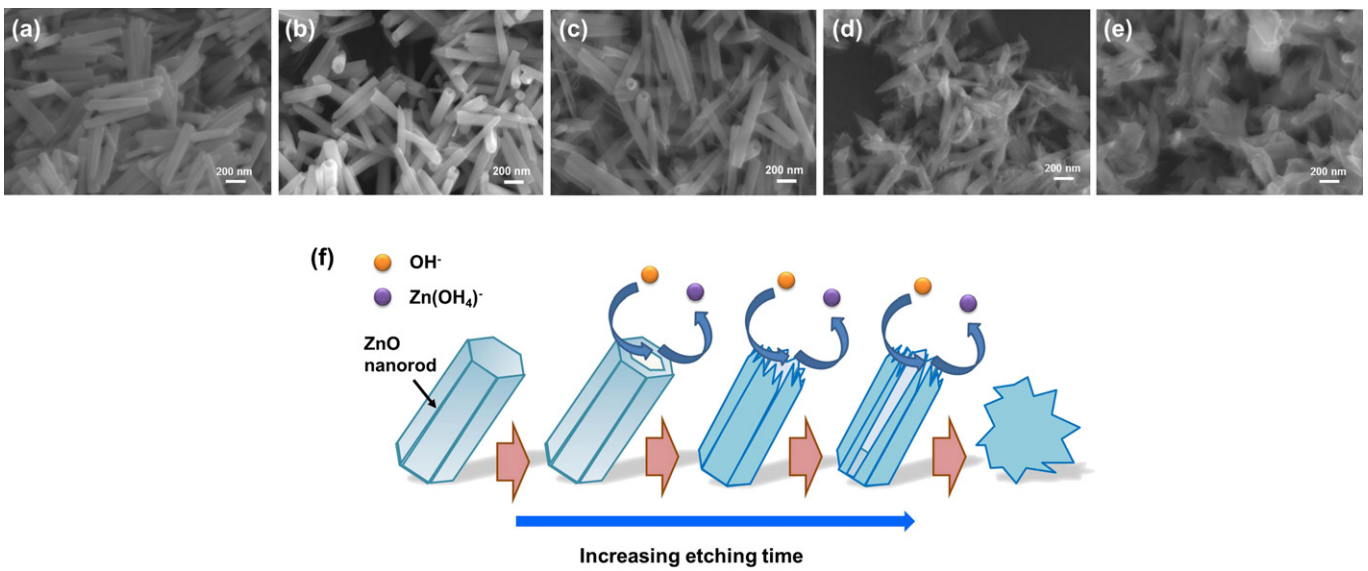

Fig. 4. Morphologies of the ZnO nanostructure obtained after etching ZnO nanorods for (a) 0 h, (b) 3 h, (c) 6 h, (d) 14 h, and (e) 24 h; (f) schematic illustration of the possible mechanism for ZnO nanosheets formation.

Please cite this article in press as: S.-L. Zhang, et al., Two-step fabrication of ZnO nanosheets for high-performance VOCs gas sensor, Current Applied Physics (2013), http://dx.doi.org/10.1016/j.cap.2012.12.021

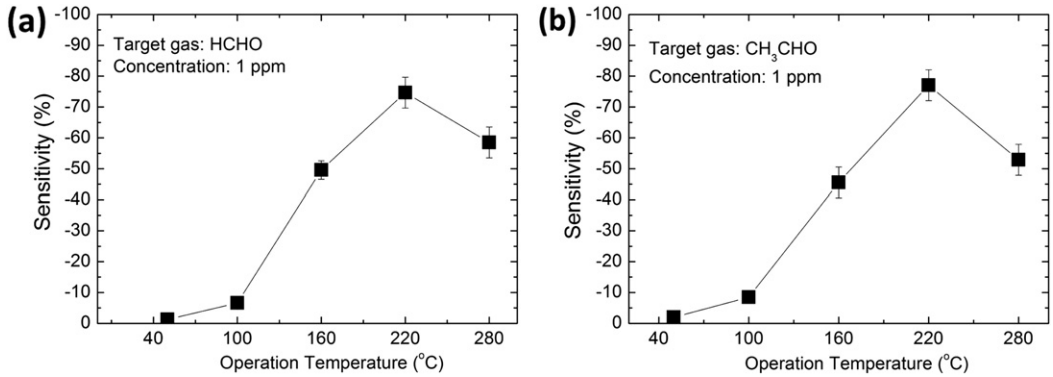

Fig. 5. Average sensitivity of the ZnO nanosheets sensor to 1 ppm of (a) formaldehyde and (b) acetaldehyde as a function of operating temperature.

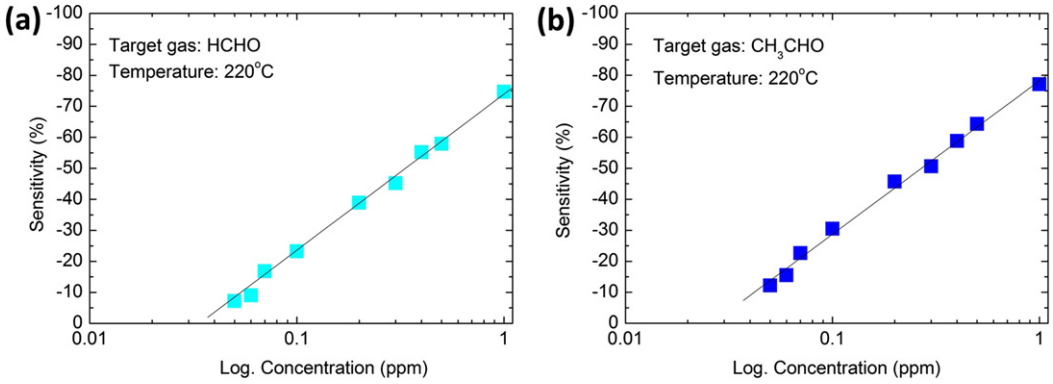

Fig. 6. Sensitivity of the ZnO nanosheets sensor as a function of concentration of (a) formaldehyde and (b) acetaldehyde.

are −75% and −77%, respectively. Therefore, the optimal operation temperature of 220 °C was chosen to further examine the characteristics of the ZnO nanosheets sensor.

The relationships between sensitivity and VOCs target gas concentrations for the ZnO nanosheets sensor are plotted in Fig. 6 at an operation temperature of 220 °C. The sensitivity linearly increases with the increase of VOCs gas concentration in the range of 50 ppb to 1 ppm. It has been reported that the saturation state may occur when all the oxygen anions absorbed on the surface of sensing material are reacted with target gas molecules [23]. In our measurement, however, there has been observed no saturation state in the full concentration range. This is because the detection range in this measurement is in a ppb level and quite low compared to other reported ZnO sensors [24,25]. Fig. 6 proves that the ZnO nanosheets sensor can detect 50 ppb of VOCs gases, and the detection limit is possibly lower than 50 ppb. Because the sensitivity of ZnO sensor is mainly determined by the interactions between the target gas molecules and the sensor surface, the performance of the sensor depends upon the available surface area of the sensor material. Our ZnO nanosheets with the plane-to-plane stacking networks possess the high surface area and efficiently avoid the agglomerated configuration, resulting in an improved sensing capability down to ppb level. It is worth noting that the ZnO nanosheets sensor exhibits a linear response to both formaldehyde and acetaldehyde in full detection range, which suggests the nanosheets sensor can serve as a promising functional sensing material for quantitative detection of VOCs gases.

The response–recovery behavior is an important characteristic that determines the performance of gas sensors. Fig. 7 shows the typical response and recovery curves of the ZnO nanosheets sensor

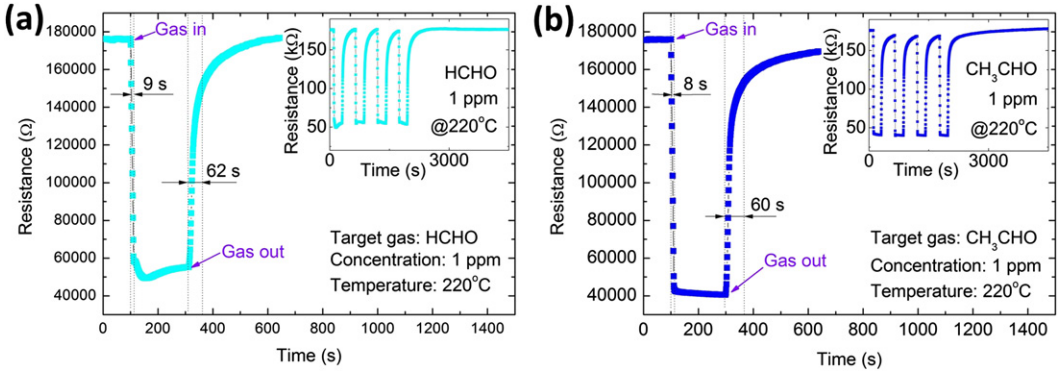

Fig. 7. Typical single-cycle response of the ZnO nanosheets sensor to 1 ppm of (a) formaldehyde and (b) acetaldehyde, the insets display multi-response characteristics.

Please cite this article in press as: S.-L. Zhang, et al., Two-step fabrication of ZnO nanosheets for high-performance VOCs gas sensor, Current Applied Physics (2013), http://dx.doi.org/10.1016/j.cap.2012.12.021

to 1 ppm of formaldehyde and acetaldehyde at the operation temperature of 220 °C. Upon exposure to the target gases, the resistance of the nanosheets sensor decreases and reaches equilibrium in short time. Once the VOCs gases are removed, the resistance quickly restores to the baseline. The response/recovery time of the ZnO nanosheets sensor to formaldehyde and acetaldehyde are evaluated to be 9/62 s and 8/60 s, respectively. Compared with other ZnO nanostructures [26–29], the ZnO nanosheets sensor has a relatively shorter response and recovery times. The response and recovery times of the sensor are generally affected by the thickness of a sensing layer, gas diffusion speed, and the reaction rate between the target gas molecule and absorbed oxygen anion, among which the gas diffusion speed is regarded as the key factor. It is believed that the existence of abundant channels and open space between the ZnO nanosheets facilitates the gas diffusion and effectively speeds up the response and recovery processes. In addition, the insets in Fig. 7 display the repeated responses of the nanosheets sensor to formaldehyde and acetaldehyde, revealing that the sensor has excellent repeatability of sensing the VOCs gases.

4. Conclusion

In summary, large-scale production of dispersed single-crystalline ZnO nanosheets was achieved using a two-step fabrication method consisting of sonochemical process and chemical etching treatment. The obtained ZnO nanosheets exhibited thickness of tens of nanometers and size of several hundred nanometers. The formation of the sheet-like morphology was attributed to the preferential etching of defect-rich parts in ZnO nanorods. The ZnO nanosheets sensor showed high sensitivity to formaldehyde and acetaldehyde with detection limit lower than 50 ppb at the optimal operation temperature of 220 °C. The high sensitivity and ppb-level detection limit were ascribed to the large specific surface area and less agglomerated configuration of the ZnO nanosheets. Furthermore, ZnO nanosheets sensor exhibited a linear response to formaldehyde and acetaldehyde in the concentration range from 50 ppb to 1 ppm, and its response and recovery times to the respective gases were around 10 s and 1 min, suggesting that the ZnO nanosheets are excellent sensing material for practical VOCs gas sensors.

Acknowledgment

This work was supported by Priority Research Centers Program through the National Research Foundation of Korea (NRF) funded by the Ministry of Education, Science and Technology (2009-0093823)

References

[1] T. Seiyama, A. Kato, K. Fujiishi, M. Nagatani, Anal. Chem. 34 (1962) 1502.
[2] A. Hoel, L.F. Reyes, P. Heszler, V. Lantto, C.G. Granqvist, Curr. Appl. Phys. 4 (2004) 547.
[3] R.C. Pawar, J.S. Shaikh, S.S. Suryavanshi, P.S. Patil, Curr. Appl. Phys. 12 (2012) 778.
[4] L.A. Patil, M.D. Shinde, A.R. Bari, V.V. Deo, Curr. Appl. Phys. 10 (2010) 1249.
[5] H. Kim, J.Y. Moon, H.S. Lee, Electron. Mater. Lett. 7 (2011) 59.
[6] S.H. Lee, H.J. Lee, H. Shiku, T. Yao, T. Matsue, Electron. Mater. Lett. 8 (2012) 511.
[7] J. Park, J. Moon, S. Lee, S. Lim, T. Zyung, Curr. Appl. Phys. 9 (2009) S210.
[8] C. Liewhiran, S. Phanichphant, Curr. Appl. Phys. 8 (2008) 336.
[9] Y. Liu, J. Dong, P.J. Heskethb, M. Liu, J. Mater. Chem. 15 (2005) 2316.
[10] Z. Jing, J. Zhan, Adv. Mater. 20 (2008) 4547.
[11] J. Li, H. Fan, X. Jia, J. Phys. Chem. C 114 (2010) 14684.
[12] J. Liu, Z. Guo, F. Meng, T. Luo, M. Li, J. Liu, Nanotechnology 20 (2009) 125501.
[13] L. Zhang, J. Zhao, H. Lu, L. Li, J. Zheng, H. Li, Z. Zhu, Sens. Actuators B 161 (2012) 209.
[14] M. Chen, Z. Wang, D. Han, F. Gu, G. Guo, J. Phys. Chem. C 115 (2011) 12763.
[15] C. Jia, S. Batterman, C. Godwin, Atmos. Environ. 42 (2008) 2083.
[16] L. Vayssieres, K. Keis, A. Hagfeldt, S. Lindquist, Chem. Mater. 13 (2001) 4395.
[17] S. Zhang, H. Byun, J. Lim, J. Huh, W. Lee, IEEE Sens. J. 12 (2012) 3149.
[18] S.L. Zhang, B.H. Cho, J.B. Yu, J.O. Lim, H.G. Byun, J.S. Huh, Sens. Lett. 9 (2011) 374.
[19] F. Li, Y. Ding, P.X. Gao, X.Q. Xin, Z.L. Wang, Angew. Chem. 116 (2004) 5350.
[20] S. Zhang, B. Cho, D. Lee, J. Lim, J. Huh, J. Nanosci. Nanotechnol. 12 (2012) 1521.
[21] S. Zhang, B. Cho, J. Yu, J. Lim, H. Byun, D. Lee, J. Huh, Sens. Lett. 9 (2011) 856.
[22] S. Zhang, J. Lim, J. Huh, W. Lee, IEEE Sens. J. 12 (2012) 3143.
[23] P. Sun, Y. Cao, J. Liu, Y. Sun, J. Ma, G. Lu, Sens. Actuators B 156 (2011) 779.
[24] Z. Bai, C. Xie, M. Hu, S. Zhang, Phys. E 41 (2008) 235.
[25] B. Li, Y. Wang, Superlattice Microstruct. 49 (2011) 433.
[26] D. Calestani, M. Zha, R. Mosca, A. Zappettini, M.C. Carotta, V. Di Natale, L. Zanotti, Sens. Actuators B 144 (2010) 472.
[27] Y. Lv, C. Li, L. Guo, F. Wang, Y. Xu, X. Chu, Sens. Actuators B 141 (2009) 85.
[28] Y. Tian, J. Li, H. Xiong, J. Dai, Appl. Surf. Sci. 258 (2012) 8431.
[29] C. Chang, S. Hung, C. Lin, C. Chen, E. Kuo, Thin Solid Films 519 (2010) 1693.

Please cite this article in press as: S.-L. Zhang, et al., Two-step fabrication of ZnO nanosheets for high-performance VOCs gas sensor, Current Applied Physics (2013), http://dx.doi.org/10.1016/j.cap.2012.12.021